RESEARCH ARTICLE

An in vivo comparison of the DREAM sequence with current RF shim technology

Kay Nehrke · Alois M. Sprinkart · Peter Börnert

Abstract

Object In the present study the performance of the dual refocusing echo acquisition mode (DREAM) B_1^+ mapping sequence is evaluated for RF shimming in the abdomen at 3 T and validated against existing RF shim technology.

Materials and methods In vivo experiments were performed on 19 normal volunteers using a clinical 3 T dual channel MRI system. For each volunteer three different B_1^+ mapping techniques [DREAM, actual flip angle imaging (AFI) and saturated double angle method (SDAM)] were employed for RF shimming of the liver and to subsequently assess the quality of the obtained RF shim settings in terms of the achieved B_1^+ homogeneity and accuracy of the mean B_1^+.

Results DREAM-based B_1^+ calibration led to an average homogeneity improvement of 39.1 % (AFI = 38.7 %, SDAM = 38.1 %) and a mean B_1^+ of 90.9 % of the prescribed B_1^+ (AFI = 88.9 %, SDAM = 92.0 %). The duration of the B_1^+ calibration scan was reduced from 30 s (AFI) and 15 s (SDAM) to 2.5 s (DREAM).

Conclusion DREAM accelerates RF shimming of the liver by an order of magnitude without compromising RF shimming performance.

Keywords B_1 mapping · RF shimming · High-field MRI · Parallel transmission

K. Nehrke (✉) · P. Börnert
Philips Research Laboratories, Röntgenstraße 24-26,
22335 Hamburg, Germany
e-mail: kay.nehrke@philips.com

A. M. Sprinkart
Department of Radiology, University of Bonn, Bonn, Germany

A. M. Sprinkart
Institute of Medical Engineering, Ruhr-University Bochum,
Bochum, Germany

P. Börnert
Leiden University Medical Center, Leiden, The Netherlands

Introduction

High-field MRI ($\geq$3 T) is prone to B_1^+ inhomogeneities in the body resulting from the dielectric shortening of the RF wavelength. Advanced MRI systems can address these problems by RF shimming based on parallel RF transmission [1–4]. Thus, significant improvements in diagnostic image quality have been obtained by RF shimming for body MRI applications at 3 T with, for example, the liver as the target anatomy [5]. However, RF shimming typically has to be performed in a patient-specific manner requiring an additional calibration scan where B_1^+ maps of the individual transmit coil elements are measured. Most B_1^+ mapping techniques determining the transmit field from the magnitudes [6–20] or phases [21, 22] of two or more acquired images are relatively slow. Therefore, depending on the employed B_1^+ mapping technique multi-channel B_1^+ calibration in the body may take several long breath-holds which has a negative impact on work flow and patient comfort.

The recently introduced ultra-fast DREAM B_1^+ mapping sequence allows RF shimming of a multi-transmit system to be performed in a few seconds [23] thus representing an attractive alternative to current RF shim technology. The general potential of the DREAM technique has been demonstrated extensively at different field strengths and for different anatomies in various studies [23–25].

It is the aim of the present study to provide a careful evaluation of the DREAM approach with respect to RF shimming on a clinical dual channel MRI system. For this purpose a DREAM B_1^+ calibration scan protocol is tailored for a liver MRI, which represents one of the important body MRI applications at 3 T. Furthermore, DREAM RF shimming performance is validated against two well-established B_1^+ mapping sequences, i.e., AFI [17] and SDAM [15], in an extensive in vivo study on 19 subjects.

Methods

MRI system and RF coils

A 3 T clinical MRI scanner (Ingenia, Philips Healthcare, Best, The Netherlands) equipped with a dual-channel Tx/Rx body coil was used. The two linear modes of the body coil are driven by two independent RF amplifiers and RF waveform generators. For the present study the standard RF shimming functionality of the system was used, applying RF pulses with individually adjustable complex weight factors for the two transmit channels. In the following the term "quadrature excitation" is used to refer to weight factors equal to "1," resulting in an equal magnitude and phase of the circular transmit field components of the two channels, $B_{1,ch1}^+$ and $B_{1,ch2}^+$, in the centre of the empty coil.

B_1^+ mapping sequences

For B_1^+ mapping three different techniques were applied, AFI, SDAM and DREAM, where the first two were provided as a standard functionality by the scan software of the MRI system employed. For the DREAM approach the sequence implementation and B_1^+ map reconstruction as previously described [23–25] has been used as a research software patch. The DREAM sequence employs a STEAM preparation module for B_1^+ encoding and a low-angle pulse train for the quasi-simultaneous acquisition of free-induction decay (FID) and stimulated echo (STE) signals as gradient-recalled echoes under a single readout gradient lobe separated in time by appropriate gradient encoding. The flip angle α of the STEAM preparation module is derived from the ratio of the FID and STE signals (I_{STE}, I_{FID}) according to:

$$\alpha = \arctan \sqrt{2 I_{STE}/I_{FID}} \tag{1}$$

In this work the "STE first" DREAM sequence version was used (cf. Fig. 1 in Ref. [24]) because it generally allows shorter repetition times (TR) of the imaging sequence than the "FID first" version. The echo times were adjusted to achieve spectral encoding times of 2.3 ms (i.e.,

water-fat in-phase at 3 T) for both STE and FID gradient echoes. The "STE first" version was favored over the fully T_2^* (including T_2) compensated "STE* first" version based on the *virtual* STE because of the more relaxed timing of the STEAM preparation module, resulting in an increased flexibility of the sequence.

Slice profile imperfections potentially impairing the accuracy of B_1^+ mapping [26] were addressed for all three approaches. For AFI [17] 3D spatial encoding was performed using only the central slice of the imaging slab for RF shimming. For SDAM [15] non-selective block-shaped RF pulses were used for RF excitation, and hence B_1^+ encoding, while slice-selective Sinc-Gaussian-shaped refocussing pulses were employed for the applied turbo spin echo (TSE) readout. For DREAM non-selective block-shaped RF pulses were used for STEAM B_1^+ encoding and slice-selective Sinc-Gaussian-shaped RF pulses for gradient echo readout [23, 24].

B_1^+ calibration scans and RF shimming

The three B_1^+ mappers considered were first used as B_1^+ calibration scans to supply complex B_1^+ (AFI) maps of the two transmit channels for RF shimming. For this purpose, the B_1^+ magnitude was determined from the underlying source images according to the B_1^+ encoding principle of the individual techniques [cf. Eq. (1) for DREAM] and the relative transmit phase was directly adopted from one of the source images. The RF shimming routine employed estimates the superposed B_1^+ as a function of a global scale factor f and the relative gain g and phase φ between the two transmit channels,

$$B_{1,(g,\varphi)}^+(\mathbf{r}) = f \cdot \left(B_{1,ch1}^+(\mathbf{r}) + e^{i\varphi + g \cdot \ln(10)/20} B_{1,ch2}^+(\mathbf{r}) \right) \tag{2}$$

where the gain is given in decibels, which explains the divisor 20 in the formula. The B_1^+ inhomogeneity expected for certain (g, φ) values is determined in terms of the coefficient of variation (CV) defined as the ratio of the standard deviation σ to the mean μ of the superposed B_1^+ field:

$$CV_{(g,\varphi)} = \frac{\sigma(B_{1,(g,\varphi)}^+(\mathbf{r}))_{\mathbf{r} \in M}}{\mu(B_{1,(g,\varphi)}^+(\mathbf{r}))_{\mathbf{r} \in M}} \tag{3}$$

where M denotes the shim mask, defining the set of valid pixels (or voxels) used for RF shimming. The shim mask is derived from a user-selected region of interest (ROI) and from an intensity-based threshold. The latter identifies B_1^+ measures likely degraded by insufficient signal (e.g., air, lungs, bowels) or vanishing B_1^+ by their low intensity in the underlying source images. From Eq. (3) the optimum gain and phase values are determined by a SAR-

constrained exhaustive search in the 2D (g, φ) parameter space (about 10,000 grid search points),

$$(g, \varphi)_{\text{opt}} = \underset{g,\varphi \in S}{\arg\min}\{CV_{(g,\varphi)}\} \qquad (4)$$

where S denotes the set of shim values allowed by the SAR model of the system. Finally, to meet the target B_1^+ the global gain factor f is determined from the ratio of the nominal field, $B_{1,\text{nom}}^+$ and the predicted mean field, μ, according to

$$f_{(r,\varphi)} = \frac{B_{1,\text{nom}}^+}{\mu(B_{1,(r,\varphi)}^+)_{\mathbf{r} \in M}} \qquad (5)$$

Experimental assessment of RF shim settings

In a second step the three B_1^+ mappers considered were used for direct experimental assessment of the RF shim settings (f, g, φ) obtained from the different B_1^+ calibration scans by acquiring RF shimmed B_1^+ maps. The CV of the measured B_1^+ maps was determined as an inhomogeneity measure and the mean B_1^+ value μ, given in percent of the nominal B_1^+, was considered as a measure for the accuracy of the B_1^+ field. For comparison additional B_1^+ maps were acquired using default quadrature transmission. To improve statistics and facilitate comparison each RF shim setting was assessed by all three B_1^+ mapping methods. Moreover, the CV values measured in B_1^+ mapping scans were compared with the CV values predicted by the calibration scans [cf. Eq. (3)] to check the self-consistency of the different methods.

The homogeneity improvement by RF shimming, in the following dubbed ζ, was quantified as:

$$\zeta[\%] = 100 \cdot \left(1 - \frac{CV_{\text{shimmed}}}{CV_{\text{quad}}}\right) \qquad (6)$$

where CV_{shimmed} and CV_{quad} indicate the B_1^+ inhomogeneity of the B_1^+ maps acquired with RF shimmed or quadrature transmission, respectively. Hence, $\zeta = 0\ \%$ corresponds to no homogeneity improvement at all and $\zeta = 100\ \%$ corresponds to a perfectly uniform B_1^+ map.

In vivo experiments

Experiments were performed on 19 normal volunteers (18 males, 1 female, min/average/max age = 31/42/58 years, body length = 169/185/198 cm, weight = 56/81/110 kg). All human studies were approved by the appropriate ethics committee and have therefore been performed in accordance with the ethical standards laid down in the 1964 Declaration of Helsinki and its later amendments. All volunteers gave their informed consent prior to their inclusion in this study. The volunteer group covers a reasonable range of patient sizes with a body mass index (BMI) from 20 to 30.

For each subject the three B_1^+ mappers were employed for B_1^+ calibration and B_1^+ homogeneity assessment as described in the previous section. Hence, the examination included three B_1^+ calibration scans and twelve B_1^+ mapping scans (see workflow diagram, Fig. 1a).
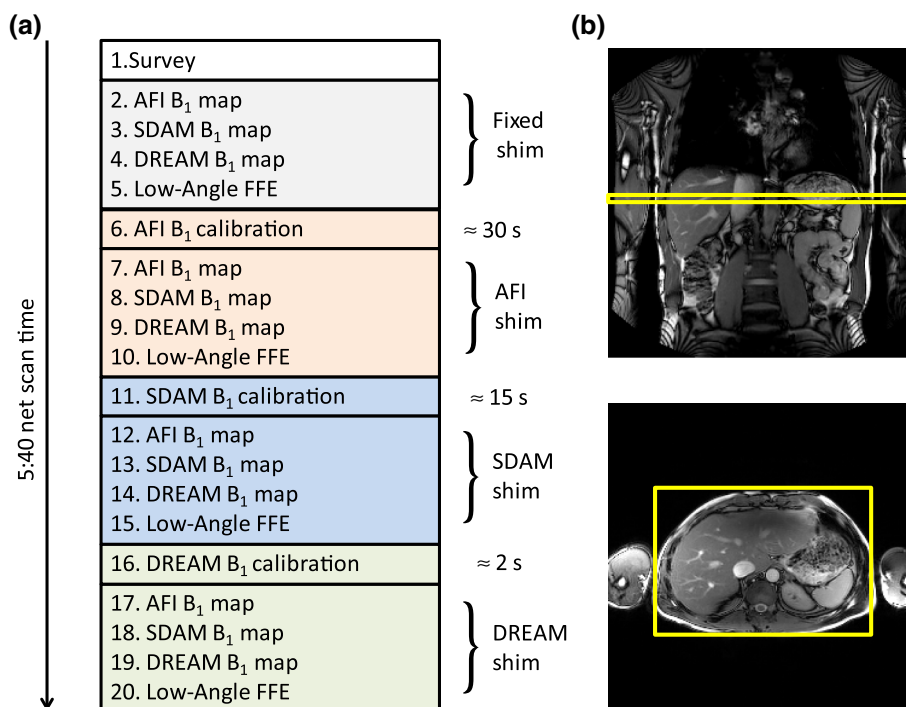
Protocol parameters of the employed calibration scans were:

1. AFI: 3D acquisition, FOV = $530 \times 464 \times 24$ mm^3, measured voxel size = $8.3 \times 10.1 \times 8$ mm^3, TR$_1$/TR$_2$/TE = 20/100/2.3 ms, nominal flip angle = 60°, whole body SAR level = 0.5 W/kg, pixel/readout bandwidth (BW) = 0.38/24.17 kHz, scan time = 31.4 s, breath-holds = 2.

2. SDAM: 2D acquisition, FOV = 530×464 mm^2, slice thickness = 20 mm, measured pixel size = 8.3×10 mm^2, TR/TE = 755/40 ms, TSE factor = 23, nominal excitation flip angle $\alpha/2\alpha$ = 130°/260°, whole body SAR level = 2.2 W/kg, pixel/readout BW = 0.22/14.17 kHz, scan time = 15.1 s, breath-holds = 1.

3. DREAM: 2D acquisition, FOV = 530×464 mm^2, measured pixel size = 8.3×8.3 mm^2, slice thickness = 20 mm, TR/TE$_{\text{STE}}$/TE$_{\text{FID}}$ = 3.8/1.1/2.3 ms, nominal imaging/STEAM flip angle = 20°/100°, imaging/STEAM RF pulse duration = 0.6/0.4 ms, whole body SAR level = 0.1 W/kg, pixel/readout BW = 0.16/10.28 kHz, shot duration = 0.2 s, shot delay = 2 s, scan time = 2.4 s, breath-holds = 1.

Prior to B_1^+ calibration the standard transmitter calibration of the system was performed on a central slice. Therefore, the indicated nominal flip angles that refer to quadrature excitation overestimate the actual flip angles in the calibration scan by roughly a factor of two because, in actuality, only one single channel, instead of dual channel transmission, is used. The selected AFI and SDAM calibration scan protocols had been optimized and approved by the manufacturer and hence were applied without further modification. The DREAM protocol was tailored and optimized in a pre-study to this work. The delay of 2 s between the acquisition of the two DREAM B_1^+ maps was introduced to avoid saturation effects potentially degrading the accuracy of the method [24].

For the acquisition of the RF shimmed and quadrature B_1^+ maps the calibration scan protocols were used as a template and adapted accordingly. The nominal flip angles were set to 50° (AFI), 65° (SDAM) and 15°/65° (DREAM), individually adjusting to the proper working ranges of the methods. All scans were performed in transversal orientation approximately intersecting the centre of the liver (Fig. 1b). For the shimmed acquisitions a user-selected B_1^+ shim volume was positioned tightly around the torso to exclude the arms from the RF shim ROI used by the RF shimming routine, illustrated also in Fig. 1b.

Fig. 1 Workflow and scan geometry. The employed scan protocol is shown schematically (**a**). For simplicity the scan order was not varied (pseudo-randomized) throughout the study. The *yellow frames* shown in (**b**) indicate the region of interest used for RF shimming

(a)

5:40 net scan time

1.Survey

| 2. AFI B$_1$ map |
| 3. SDAM B$_1$ map |
| 4. DREAM B$_1$ map |
| 5. Low-Angle FFE |

Fixed shim

6. AFI B$_1$ calibration

≈ 30 s

| 7. AFI B$_1$ map |
| 8. SDAM B$_1$ map |
| 9. DREAM B$_1$ map |
| 10. Low-Angle FFE |

AFI shim

11. SDAM B$_1$ calibration

≈ 15 s

| 12. AFI B$_1$ map |
| 13. SDAM B$_1$ map |
| 14. DREAM B$_1$ map |
| 15. Low-Angle FFE |

SDAM shim

16. DREAM B$_1$ calibration

≈ 2 s

| 17. AFI B$_1$ map |
| 18. SDAM B$_1$ map |
| 19. DREAM B$_1$ map |
| 20. Low-Angle FFE |

DREAM shim

(b)

For complementary assessment of the RF shimming performance in addition to the B$_1^+$ mapping scans a 3D dual echo Dixon FFE scan (FOV = 520 × 359 × 120 mm^3, measured voxel size = 1.9 × 1.9 × 5 mm^3, TE$_1$/TE$_2$/TR = 1.1/2.0/3.2 ms, flip angle = 5°, whole body SAR level = 0.2 W/kg, WFS = 0.24 pixel, scan time = 16 s, breath-holds = 1) was performed for each shim set. This low-tip angle scan was chosen as an additional and independent visual test for the B$_1^+$ homogeneity because it is sensitive to B$_1^+$-induced tip angle variations that can lead to significant contrast changes and loss of image quality in such a diagnostic protocol. For each subject the water image of the central slice was analyzed and scored with respect to the B$_1$ homogeneity [accordingly, 1 (excellent) to 5 (very bad)] by two different experienced readers.

The net scan time of the overall examination was 5:40 min (cf. Fig. 1a). The measured B$_1^+$ maps were exported from the scanner database after the examination and stored along with the corresponding RF shim sets for subsequent evaluation using in-house image processing tools written in Java.

Results

Experimental issues

For all volunteers the complete examination could be carried out in about 10–15 min. The long 15-sec breath-holds,

required for the AFI and SDAM calibration scans, were perceived as stressful by about 20 % of the volunteers. For one volunteer (#1) the AFI scans (calibration maps and shimmed maps as well) were degraded by respiratory motion (see detailed results below). Moreover, about 30 % of the volunteers mentioned a noticeable warming by the SDAM sequence, which can be explained by the higher, but still well in-spec, SAR level of this TSE-based scan.

B$_1^+$ calibration scans and RF shimming

Figure 2 shows the transmit channel sensitivities measured using the three different B$_1^+$ calibration methods and the employed shim mask for two exemplary volunteers (#13 and #1). All calibration methods reveal the well-known diagonal shading pattern for Tx channel #1, typical for this coil configuration in abdominal MRI at 3 T [25]. The AFI maps show a higher background inhomogeneity from noise and artefacts than the SDAM and DREAM maps which was observed for most of the volunteers in this study. Particularly, the AFI maps of volunteer #1 are degraded by respiratory motion artifacts. The intensity-based masks that exclude B$_1^+$ measures degraded by insufficient signal or vanishing B$_1^+$ are similar for all three methods. The user-selected shim volume additionally excludes the arms from the shim ROI.

Figure 3a, b show the B$_1^+$ inhomogeneity predicted from the three calibration scans for the same volunteers (#13 and #1). The 2D plots show the expected *CV* maps as a function of the gain and phase between the two channels

Fig. 2 B_1^+ calibration scans of selected volunteers. Transmit sensitivities of the two transmit channels (*top*: channel #1; *centre*: channel #2; *bottom*: shim mask) as measured by the three calibration sequences (*left*: AFI; *centre*: SDAM; *right*: DREAM) are shown for two volunteers (#13 and #1). The *colored frames* (*top*) indicate the user-selected shim volume excluding the arms from the shim mask (*bottom*). For volunteer #1 ghosting artifacts from respiratory motion are noticeable (*arrow*). Note that the AFI and SDAM scan protocols employ interpolation to increase resolution in the reconstructed maps
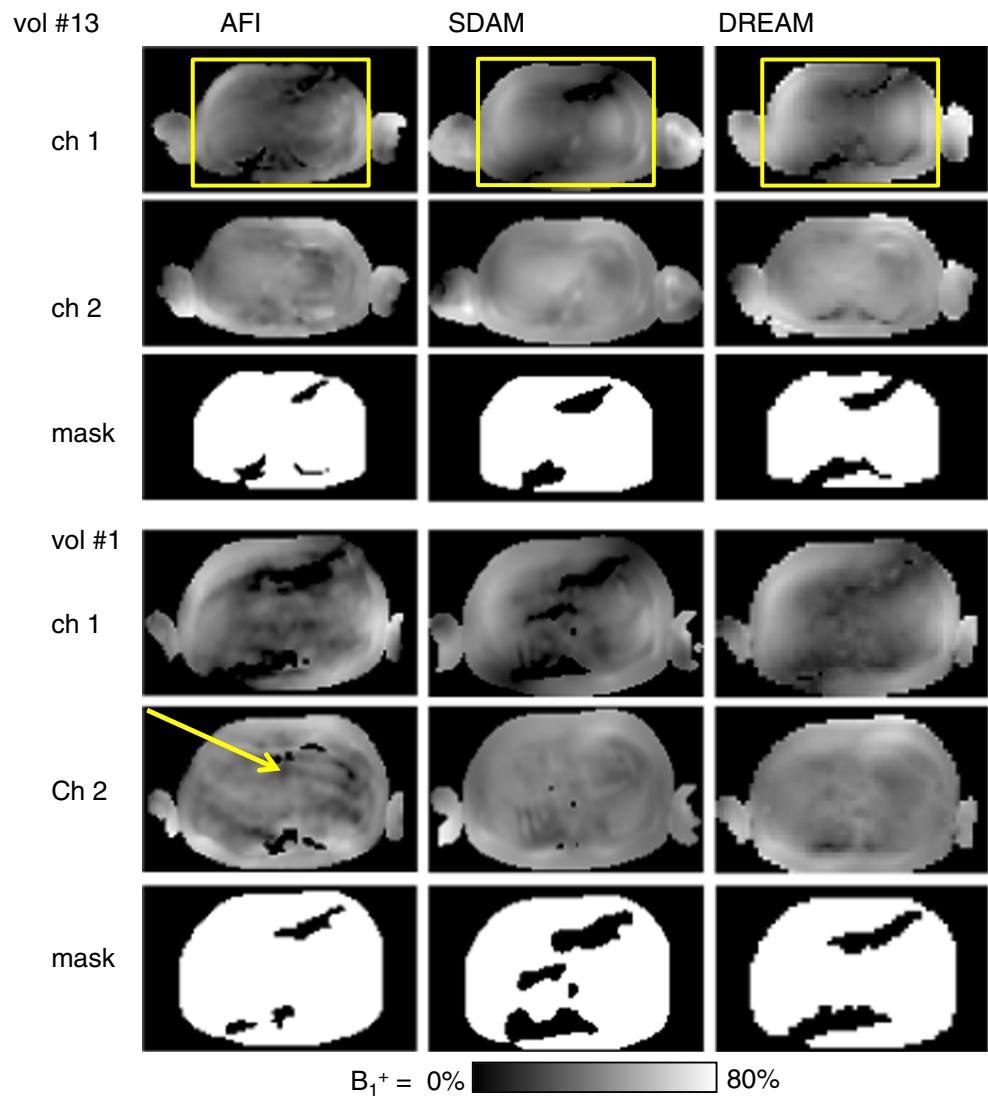
[cf. Eq. (3)]. The centre of the plots corresponds to quadrature shim settings (i.e., zero gain and phase between channels). All plots show a maximum in the left centre and a minimum in the upper centre of the 2D parameter space. The minimum corresponds to the optimum shim setting leading to the most uniform B_1^+ field and will be in the focus of the analysis in the following. Minor deviations between the different mapping methods are visible leading to slightly different predictions for the optimal RF shim setting. Despite the motion artifacts in the AFI calibration maps of volunteer #1 (cf. Fig. 2), the resulting *CV* map is rather smooth and regular. Comparison between the two subjects shows systematic differences in the optimal shim settings affecting mainly the phase offset between the two Tx channels.

Figure 4 summarizes the optimal shim settings determined from the different calibration scans for all volunteers. For most volunteers the optimum gain and phase

between the two channels is about 7–10 dB and 30°–50°, respectively. For two volunteers (#1, #19) a significantly smaller phase between 0°–25° was determined by all calibration methods.

RF shimmed B_1^+ mapping scans

Figure 5 shows the B_1^+ maps measured under different shimming conditions for one volunteer (#13). Each of the four RF shim settings (quadrature, AFI, SDAM, DREAM) was evaluated by each of the three B_1^+ mapping techniques (AFI, SDAM, DREAM) resulting in twelve B_1^+ maps.

For quadrature RF shims the typical shading artifacts are observed in the anterior and posterior torso [5]. A noticeable reduction of the B_1^+ inhomogeneity is observed for all calibration scans and all mapping scans resulting in a strongly reduced *CV*. Moreover, the deviation of the mean B_1^+ from the nominal B_1^+ is reduced. The AFI maps show
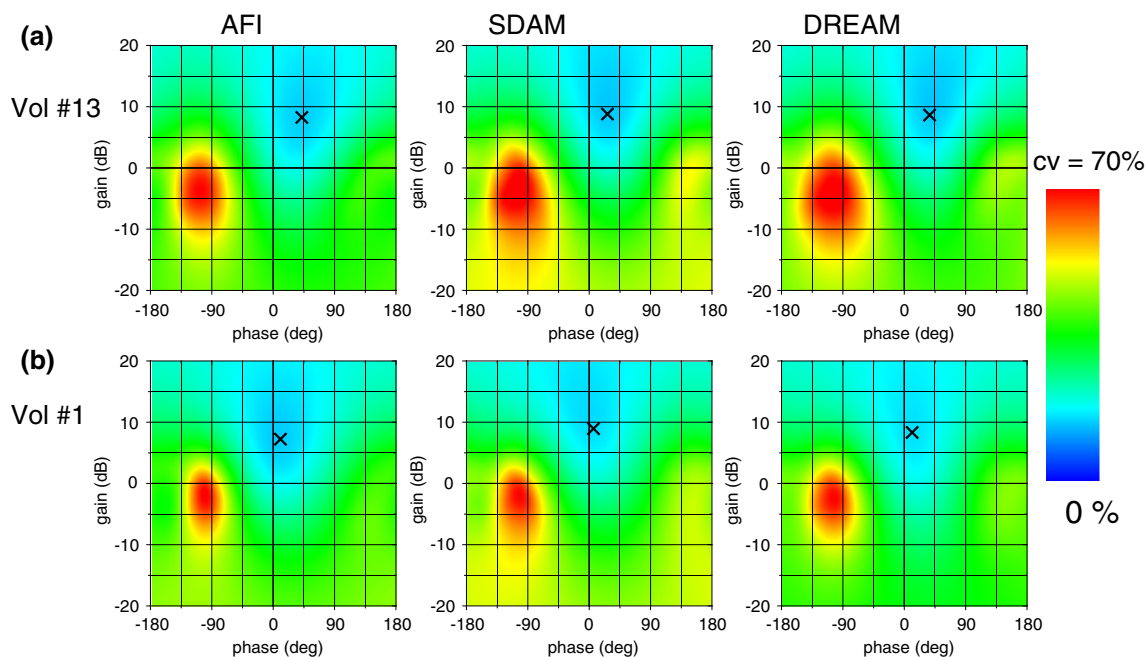
Fig. 3 CV maps. The expected CV of the torso B_1^+ is shown as a function of gain and phase between the two Tx channels for two selected volunteers. CV was predicted from the measured calibration scan (*left*: AFI; *centre*: SDAM; *right*: DREAM) according to Eq. (3). The crosses indicate the optimum RF shim settings yielding the minimum CV
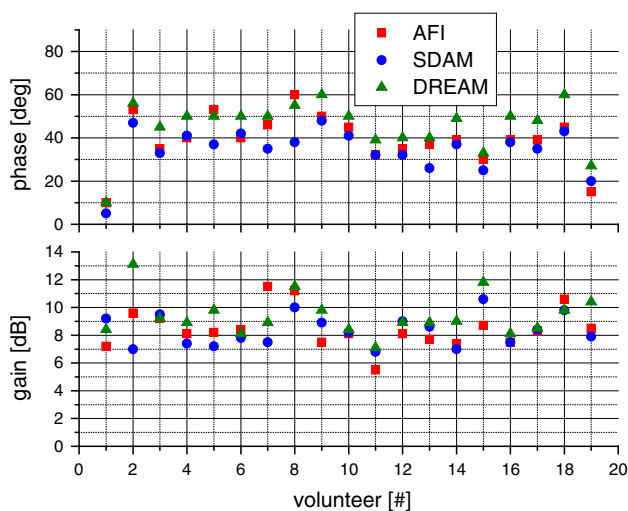

Fig. 4 RF shim settings. Optimal gain and phase between the two transmit channels is shown for the different volunteers and calibration scans

again an increased background inhomogeneity from noise resulting in larger CV values. Similar to the B_1^+ maps the quadrature low-angle FFE images confirm these findings showing strong shading that is strongly reduced after RF shimming.

Figure 6 summarizes CV values measured by the different B_1^+ maps for the different RF shim settings for all 19

volunteers. For fixed shims the CV varies between 20 and 35 % and is reduced to 10–25 % after RF shimming. Table 1 summarizes the corresponding results averaged over the volunteer group. The AFI B_1^+ maps show a higher average CV value than the SDAM and DREAM B_1^+ maps which is probably due to the higher noise-related artifact level observed for the employed AFI scan protocol. For one volunteer (#1) ghosting artifacts in the shimmed AFI maps resulted in an apparent *increase* of the CV after shimming. These obviously erratic data were excluded from further evaluation and, hence, are not shown in the figure. The CV averaged over all subjects and over the three B_1^+ mappers is about 27 % for quadrature excitation and about 17 % for RF shimmed excitation regardless of the employed calibration method; this indicates similar RF shimming performance of the three methods. This is supported by scoring of the low-angle FFE images with an average score of 3.2 for quadrature excitation and about 1.5 for RF shimmed excitation (cf. Table 1). The plots show also the CV values predicted from the B_1^+ calibration scans for comparison. The DREAM method shows the best accordance between predicted and measured CV values with a mean deviation of 1.1 % over the whole volunteer group (Table 2). In comparison, for AFI and SDAM a mean deviation of 2.3 and 3.3 %, respectively, is observed. This indicates that the DREAM data show the best self-consistency.

Figure 7 shows the improvement in B_1^+ homogeneity, ζ, for the different calibration techniques [cf. Eq. (6)]. For
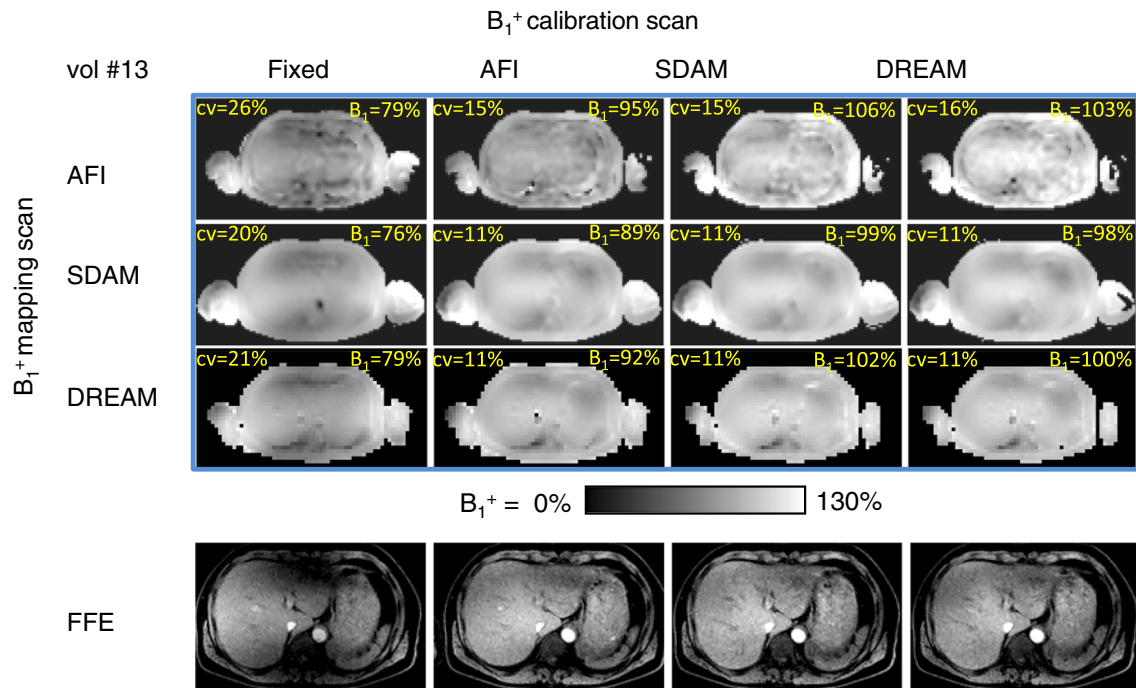
Fig. 5 RF Shimmed B_1^+ maps. B_1^+ maps measured with different techniques (*top to bottom*: AFI, SDAM, DREAM) and with RF shims derived from different calibration scans (*left to right*: quadrature, AFI, SDAM, DREAM) are shown. *CV* and the mean B_1^+ (in % of the nominal B_1^+) in the torso are shown as insets in the images. In addition, low-angle, water-only FFE images are shown for the different shim sets (*bottom row*) revealing the impact of B_1^+ shimming

Fig. 6 B_1^+ homogeneity. *CV* of the torso B_1^+ maps is plotted for the different volunteers. Four different shim settings (quadrature: *top left*; AFI: *top right*; SDAM: *bottom left*; and, DREAM: *bottom right*) are evaluated by three B_1^+ mapping techniques (AFI: *solid squares*; SDAM: *solid circles*; DREAM: *solid triangles*). In addition, *CV* values predicted by the different calibration scans are shown as *open symbols*. The lines are guides for the eyes. For all calibration methods the *CV* is significantly reduced compared to quadrature excitation
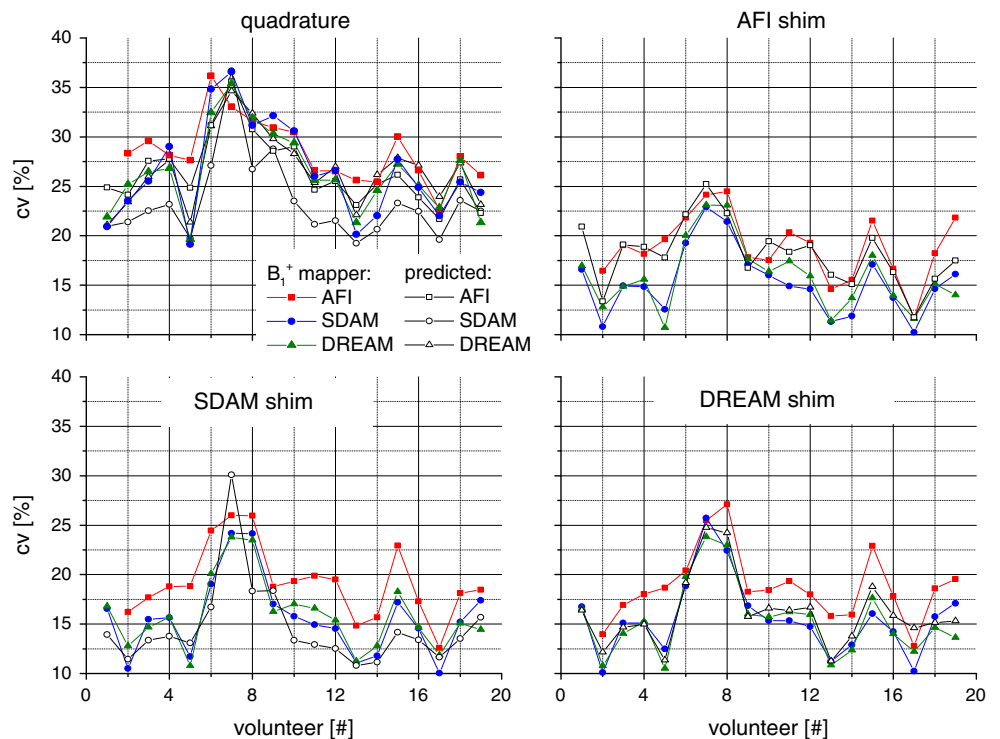
clarity of presentation improvement was averaged over the three B_1^+ mappers. Dependent on the volunteer, an improvement between 20 and 55 % is achieved. For the individual subjects differences between the calibration methods are observed but without a strong and clear overall trend favoring one of the methods. Averaged over all

Table 1 RF shimming performance averaged over volunteers

RF shim settings

	Quadrature	AFI	SDAM	DREAM
B_1^+ mapper				
AFI				
CV (%)	28.5 ± 3.2	18.8 ± 3.3	19.2 ± 3.7	18.8 ± 3.6
μ (%)	66.7 ± 9.7	90.9 ± 6.1	95.2 ± 8.0	93.8 ± 7.3
ζ (%)	0	34.1 ± 8.5	33.1 ± 7.7	34.3 ± 9.1
SDAM				
CV (%)	26.5 ± 4.9	15.3 ± 3.4	15.6 ± 3.9	15.6 ± 3.8
μ (%)	64.4 ± 8.7	87.9 ± 5.0	90.7 ± 7.1	89.8 ± 6.3
ζ (%)	0	42.0 ± 8.0	41.1 ± 9.3	41.0 ± 9.3
DREAM				
CV (%)	26.4 ± 4.2	15.9 ± 3.5	15.9 ± 3.6	15.4 ± 3.7
μ (%)	66.2 ± 9.4	88.1 ± 5.4	90.3 ± 7.0	89.4 ± 6.2
ζ (%)	0	39.8 ± 7.3	40.0 ± 7.6	41.8 ± 8.2
Average				
CV (%)	**27.1 ± 4.2**	**16.6 ± 3.7**	**16.9 ± 3.3**	**16.6 ± 4.0**
μ (%)	**65.8 ± 9.2**	**88.9 ± 5.6**	**92.0 ± 7.6**	**90.9 ± 6.8**
ζ (%)	**0**	**38.7 ± 8.5**	**38.1 ± 8.6**	**39.1 ± 9.3**
FFE images				
score (1–5)	3.2 ± 0.5	1.6 ± 0.5	1.5 ± 0.4	1.4 ± 0.5

The B_1^+ inhomogeneity (CV), the mean B_1^+ (μ) and the homogeneity improvement (ζ) are indicated for the different B_1^+ mappers and RF shim settings. All values represent averages over the volunteer group where the given standard deviations indicate variability between subjects. The bold values at the bottom indicate the corresponding values additionally averaged over the three employed B_1^+ mappers. In addition, in the last row the average scores for the homogeneity of the low-angle FFE images are given. All data indicate a significant improvement of B_1^+ homogeneity by RF shimming. In contrast, differences between the three RF shimming techniques are small and not significant

Table 2 Self-consistency of B_1^+ mappers

	AFI	SDAM	DREAM
Quadrature	2.6	3.8	1.2
RF shimmed	1.8	2.6	0.9
Total	2.3	3.3	1.1

The mean deviation (in %) between predicted and measured CV values over the volunteer group is shown for the different B_1^+ mappers. Quadrature B_1^+ maps were synthesized from the calibration scan using zero gain and phase between the two transmit channels [cf. Eq. (3)]

volunteers almost a 40 % improvement is achieved for all methods (AFI: 38.7 %; SDAM: 38.1 %; DREAM: 39.1 %; cf. Table 1).

Figure 8 shows the mean torso B_1^+, μ, achieved for the different calibration schemes. For fixed shim settings the mean B_1^+ is between 55 and 80 %, dependent on the volunteer. B_1^+ shimming yields a mean B_1^+ between 80 and
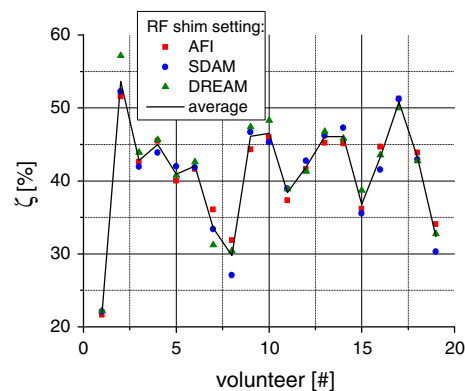

Fig. 7 B_1^+ homogeneity improvement. The improvement in B_1^+ homogeneity, ζ, is compared for the different shim sets (AFI, SDAM, DREAM). The *lines* are guides for the eyes. Deviations between the calibration methods are small compared to deviations between volunteers. On average a similar RF shimming performance is observed for all calibration methods (cf. Table 1)
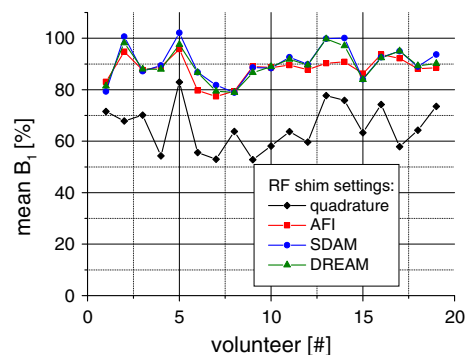

Fig. 8 B_1^+ accuracy. The mean torso B_1^+ is shown for the different volunteers and RF shim settings (given in % of the nominal B_1^+). The *lines* are guides for the eyes. All calibration methods increase the mean B_1^+ and achieve on average about 90 % of the prescribed B_1^+ (cf. Table 1)

100 %. On average RF shimming increases the mean B_1^+ from about 65 % to about 90 % (AFI: 88.0 %; SDAM: 90.5 %; DREAM: 89.6 %; cf. Table 1). Deviation from the expected 100 % may be mainly attributable to the over-tipping protection of the shimming routine, which poses a limit on the maximum B_1^+ also outside the shim ROI. Thus, for the chosen anatomy the overall B_1^+ is scaled down to reduce the relative strong fields in the arms (cf. Figs. 2, 5).

Discussion

This comprehensive in vivo study shows that the DREAM method fully matches the RF shimming performance of two established B_1^+ calibration methods (i.e., AFI and SDAM) used for RF shimming of the liver on the

employed 3 T MRI system. All calibration methods achieved about 40 % homogeneity improvement and about 90 % of the nominal B_1^+ on average. Regarding the individual volunteers slight differences were observed between the methods, however, without a clear trend favoring one of the approaches. Furthermore, differences were hardly noticeable in the low-angle FFE images. Nevertheless, the DREAM approach showed the best consistency between calibration scans and RF shimmed B_1^+ mapping scans. Deviations between the methods may be attributable to the known limitations of the individual approaches (e.g., low dynamic range, SNR, sensitivity to motion, flow, T_1, T_2, etc.), protocol trade-offs, variability in the automatically generated shim masks or physiological effects like the limited reproducibility of breath hold levels or peristaltic motion. It is difficult to analyze the impact of these different aspects separately in an in vivo study and, hence, the attained B_1^+ homogeneity was used as an integral measure for the performance of the methods. Interestingly, the generally lower B_1^+ map quality of the employed AFI calibration scan observed in this study did not lead to a noticeable degradation of RF shimming performance. A potential explanation is the considered two-channel RF shimming problem represents a highly overdetermined optimization problem where one complex number has to be determined from many measured B_1^+ values, making it robust against, for example, noise or motion artifacts in the measured data.

RF shim settings obtained in this volunteer study varied in a range of 10°–60° phase offset and 6–13 dB gain between the two transmit channels. For real patients with certain pathologic findings (e.g., ascites [5]) an even stronger variability of RF shading was reported, further underlining the need of patient-specific RF shimming. The DREAM approach allows these issues to be addressed without adding significant overhead to the examination. It is an order of magnitude faster and has a much lower SAR level than the existing techniques. Thus, patient discomfort and image quality problems related to breath holding can be reduced, which represents a strong improvement in workflow over the existing techniques. For this very first comparative study a quite conservative single-slice DREAM scan protocol has been applied with a comparatively "long" delay of 2 s between the two shots, resulting in a total scan time of 2.4 s performed in a short breath hold. This was done to facilitate a fair comparison of the methods, thus making the study design simple and establishing a baseline for the performance of the DREAM approach. Nevertheless, shorter delays are conceivable and the single-shot characteristic of the DREAM approach enables free-breathing B_1^+ mapping [27] that both could further improve the workflow towards short and hidden preparation phases.

In all volunteers of this study significant improvements in B_1^+ homogeneity were achieved after shimming. The CV maps (cf. Fig. 3) and their good accordance to the measured B_1^+ maps indicate that the calibration scans exploit the RF shimming capabilities of the employed transmit coil to a large extent.

Transmit coils with a higher channel count can further improve B_1^+ homogeneity at 3 T [28]. However, the increased complexity of such a system with respect to hardware demands, B_1^+ interferometry [29–31], RF shimming algorithms and SAR prediction has to be carefully balanced against the potential gain in RF shimming performance possible at 3 T. On the other hand, at ultra high field strength transmit field inhomogeneities will be even more pronounced [24] underlining the need for more than two transmit channels. In this respect DREAM has been shown to be applicable for multi-channel B_1^+ mapping at ultra high field strength [32].

In conclusion, for body imaging at 3 T the DREAM method is as robust as, but much faster, than current RF shim technology. Hence, the RF shimming capabilities of the employed MRI system may be fully exploited using patient-specific calibration without compromising work flow.

References

1. Hoult DI, Phil D (2000) Sensitivity and power deposition in a high-field imaging experiment. J Magn Reson Imaging 12:46–67
2. Ibrahim TS, Lee R, Baertlein BA, Abduljalil AM, Zhu H, Robitaille PM (2001) Effect of RF coil excitation on field inhomogeneity at ultra high fields: a field optimized TEM resonator. Magn Reson Imaging 19:1339–1347
3. Katscher U, Börnert P, Leussler C, van den Brink JS (2003) Transmit sense. Magn Reson Med 49:144–150
4. Zhu Y (2004) Parallel excitation with an array of transmit coils. Magn Reson Med 51:775–784
5. Willinek WA, Gieseke J, Kukuk GM et al (2010) Dual-source parallel radiofrequency excitation body MR imaging compared with standard MR imaging at 3.0 T: initial clinical experience. Radiology 256:966–975
6. van der Meulen P, van Yperen GH (1983) A novel method for rapid pulse angle optimisation. Proceedings of the 5th annual meeting of SMRM, Montreal, Canada. (Abstract 1129)
7. Carlson JW, Kramer DM (1990) Rapid radiofrequency calibration in MRI. Magn Reson Med 15:438–445
8. Klose U (1992) Mapping of the radio frequency magnetic field with a MR snapshot FLASH technique. Med Phys 19:1099–1104
9. Insko E, Bolinger L (1993) Mapping of the radio frequency field. J Magn Reson, Ser A 103:82–85
10. Akoka S, Franconi F, Seguin F, Le Pape A (1993) Radiofrequency map of an NMR coil by imaging. Magn Reson Imaging 11:437–441
11. Stollberger R, Wach P (1996) Imaging of the active B1 field in vivo. Magn Reson Med 35:246–251

12. Sled JG, Pike GB (2000) Correction for B1 and B0 variations in quantitative T2 measurements using MRI. Magn Reson Med 43:589–593

13. Fernandez-Seara MA, Song HK, Wehrli FW (2001) Trabecular bone volume fraction mapping by low-resolution MRI. Magn Reson Med 46:103–113

14. Wang J, Qiu M, Constable RT (2005) In vivo method for correcting transmit/receive nonuniformities with phased array coils. Magn Reson Med 53:666–674

15. Cunningham CH, Pauly JM, Nayak KS (2006) Saturated double-angle method for rapid B1 mapping. Magn Reson Med 55:1326–1333

16. Jiru F, Klose U (2006) Fast 3D radiofrequency field mapping using echoplanar imaging. Magn Reson Med 56:1375–1379

17. Yarnykh VL (2007) Actual flip-angle imaging in the pulsed steady state: a method for rapid three-dimensional mapping of the transmitted radiofrequency field. Magn Reson Med 57:192–200

18. Helms G, Finsterbusch J, Weiskopf N, Dechent P (2008) Rapid radiofrequency field mapping in vivo using single-shot STEAM MRI. Magn Reson Med 60:739–743

19. Volz S, Nöth U, Rotarska-Jagiela A, Deichmann R (2010) A fast B1-mapping method for the correction and normalization of magnetization transfer ratio maps at 3 T. Neuroimage 49:3015–3026

20. Chung S, Kim D, Breton E, Axel L (2010) Rapid B1+ mapping using a preconditioning RF pulse with TurboFLASH readout. Magn Reson Med 64:439–446

21. Morrell GR (2008) A phase-sensitive method of flip angle mapping. Magn Reson Med 60:889–894

22. Sacolick LI, Wiesinger F, Hancu I, Vogel MW (2010) B1 mapping by Bloch-Siegert shift. Magn Reson Med 63:1315–1322

23. Nehrke K, Börnert P (2012) DREAM—a novel approach for robust, ultrafast, multislice B(1) mapping. Magn Reson Med 68:1517–1526

24. Nehrke K, Versluis MJ, Webb A, Börnert P (2014) Volumetric B(1) (+) mapping of the brain at 7 T using DREAM. Magn Reson Med 71:246–256

25. Sprinkart AM et al. Ultrafast volumetric B1+ mapping for improved RF shimming in 3 T body MRI. J Magn Reson Imaging. 4. doi:10.1002/jmri.24438

26. Wang J, Mao W, Qiu M, Smith MB (2006) Constable RT. Factors influencing flip angle mapping in MRI: RF pulse shape, slice-select gradients, off-resonance excitation, and B0 inhomogeneities. Magn Reson Med. 56:463–468

27. Nehrke K and Börnert P.(2012) Free-breathing abdominal B1 mapping at 3 T using the DREAM approach. Proceedings of International Society for Magnetic Resonance. 20. (Abstract 1920)

28. Childs AS, Malik SJ, O'Regan DP, Hajnal JV (2013) Impact of number of channels on RF shimming at 3 T. MAGMA 26:401–410 (Epub 2013 Jan 13)

29. Brunner DO, Pruessmann KP (2009) B1(+) interferometry for the calibration of RF transmitter arrays. Magn Reson Med 61:1480–1488

30. Malik SJ, Larkman DJ, Hajnal JV (2009) Optimal linear combinations of array elements for B1 mapping. Magn Reson Med 62:902–909

31. Nehrke K, Börnert P (2010) Eigenmode analysis of transmit coil array for tailored B1 mapping. Magn Reson Med 63:754–764

32. Tse DHY, Poole MS, Magill AW, Felder J, Brenner D, and Shah NJ (2014) Encoding methods for B1+ mapping in parallel transmission systems at ultra high field. In: Proceedings of International Society for Magnetic Resonance 22. (Abstract 4336)